



Research paper

Shape and contact force estimation of continuum manipulators using pseudo rigid body models

Venkatasubramanian Kalpathy Venkiteswaran^{a,*}, Jakub Sikorski^a, Sarthak Misra^{a,b}^a Surgical Robotics Laboratory, Department of Biomechanical Engineering, University of Twente, 7500 AE Enschede, The Netherlands^b Department of Biomedical Engineering, University of Groningen and University Medical Centre Groningen, 9713 GZ Groningen, The Netherlands

ARTICLE INFO

Article history:

Received 9 November 2018

Revised 29 March 2019

Accepted 12 April 2019

Keywords:

Continuum manipulator
 Pseudo-rigid-body model
 Force estimation
 Magnetic actuation
 Surgical robotics

ABSTRACT

Accurate estimation of deformed shape and reaction forces poses a significant challenge in modeling and control of continuum manipulators interacting with their environment. This paper presents a framework for the analysis of a continuum manipulator subjected to multiple external loads using pseudo rigid body (PRB) modelling method. A PRB model with six degrees of freedom is developed, and the statics equations for a manipulator with multiple loads are presented, followed by the approach for determining the optimal model parameters. Dimensionless constants are used to enable scaling the model to manipulators of different lengths and materials. The approach is first validated by a comparison with Finite Element Analysis, and the results show a low error in estimating the tip deflection (less than 1% of the manipulator length). A magnetically-actuated manipulator driven by an array of electromagnetic coils is used for experimental validation. The optimization for a single segment of the manipulator is performed with experimental data, with an average error of 2.2 mm in calculating the tip position. An experimental setup for a manipulator with multiple loads is created by introducing displacement constraints with fixtures connected to multi-axis force sensors. The model shows good agreement with quasi-static experiments in estimating the reaction forces and predicting the deformed shape of the manipulator. The average error in force estimation is 61 mN, while the average error in estimating tip position is 2.8 mm for a manipulator length of 82 mm.

© 2019 Elsevier Ltd. All rights reserved.

1. Introduction

Continuum manipulators provide significant advantages over traditional rigid-link robots in terms of locomotion and dexterity. They are particularly useful in navigating constrained and cluttered environments due to their inherent large number of degrees of freedom [1]. These characteristics make them conducive to exploratory operations such as search and rescue. Soft and compliant manipulators utilize the deformation of elastic elements to achieve motion [2]. With compliance matching, they can be safely used in intra-operative procedures since there is little risk of tissue damage, which makes them suitable for minimally invasive surgery (MIS) [3,4].

* Corresponding author.

E-mail addresses: v.kalpathyvenkiteswaran@utwente.nl (V.K. Venkiteswaran), j.sikorski@utwente.nl (J. Sikorski), s.misra@utwente.nl (S. Misra).

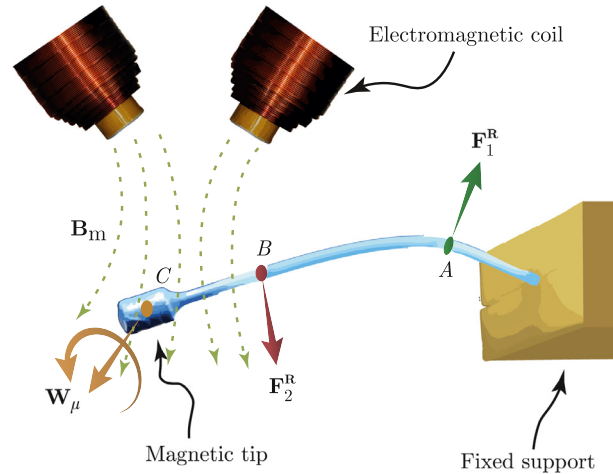


Fig. 1. A continuum manipulator subjected to multiple loads is shown. The actuation wrench ($\mathbf{W}_\mu \in \mathbb{R}^6$) is generated due to the interaction between the external magnetic field ($\mathbf{B}_m \in \mathbb{R}^3$) and the dipole at the magnetic tip (C). Displacement boundary conditions are enforced at points (A and B) along the length of the manipulator, resulting in reaction forces ($\mathbf{F}_1^R \in \mathbb{R}^3$ and $\mathbf{F}_2^R \in \mathbb{R}^3$). A framework for the analysis of continuum manipulators subjected to multiple loads using pseudo rigid body models is presented in this paper.

However, the structural redundancy (multiple degrees of freedom) of continuum manipulators renders them difficult to model and control. Accurate modeling of such systems can be challenging due to the nonlinearities arising from material properties and large deformation. Constant-curvature approximations help reduce the complexity associated with continuum motion, but are limited to specific applications [5,6]. Another approach is to utilize Cosserat rods to develop geometrically-exact models [7,8]. Previously, Tang et al. used this method for estimating the shape of catheters and guidewires including surface friction, with experimental validation for small deflections [9]. Till et al. analyzed a wire-driven parallel manipulator [10]. Force estimation in continuum devices has been traditionally limited to single loads at the tip, whereas in reality contact may occur anywhere along the manipulator length [11,12]. Recent work by Coevoet et al. and Zhang et al. has studied shape and force estimation under contact for soft manipulators using a Finite Element Method (FEM) model [13,14].

In this paper, we present a pseudo rigid body modelling approach for estimation of deflection and shape of a magnetically-actuated continuum manipulator, including environmental loads (Fig. 1). This is demonstrated through experimental validation of deflection and shape calculation in 3D for quasi-static scenarios, including estimation of contact and non-contact loads that affect the motion of the manipulator. The framework used in this work can be adapted for other soft or continuum manipulators.

Pseudo rigid body (PRB) models are numerical approximations of flexible elements with springs for capturing the compliance and rigid links for estimating the kinematics of the system [15]. PRB models can be extended to encompass a variety of mechanical deformation characteristics, and allow for simplified definitions of compliant elements to speed up computation [16]. This also enables the models to be used for real-time control through inverse kinematics equations based on rigid-body dynamics. Khoshnam et al. previously used a PRB model for analysis of planar deflection of catheters [17]. Greigarn et al. also used a PRB model for catheter analysis, but it was limited to a specific catheter design and did not include interaction with the environment or the effect of gravity [18,19]. Previous work by Roesthuis and Misra used a constant-curvature approach combined with rigid-link modeling, but was restricted to manipulators undergoing planar deformations, and subjected only to moment loads [20]. Huang et al. used a planar PRB model for analysis of a cable-driven continuum manipulator [21]. Open and closed-loop experiments were performed on a magnetic catheter by Edlmann et al., but required prior knowledge of external loads for numerical integration using Cosserat rods [22].

The PRB model presented here is generally applicable (in 3D) to manipulators made of flexible materials with a high aspect ratio (length to cross-section diameter). The framework also incorporates the response of the system to multiple external loads. This is demonstrated through the estimation of manipulator shape and contact forces with the environment, through both Finite Element Analysis (FEA) and experiments. The discussion is limited to static conditions, but the model is applicable to dynamic environments, and can handle large deformations. The model is defined with dimensionless parameters to enable it to be extended to other loading scenarios. The PRB model defines the equations of motion in a simple format that can be solved in real-time for closed-loop control. Compared to other methods in literature, the model can be fitted to a wide range of deformation characteristics even when accurate information about system properties is *a priori* unavailable.

The experiments for validating the methodology are conducted with a magnetic catheter made from a thermoplastic elastomer, for minimally invasive surgery. Magnetic actuation has the advantage of being non-contact and non-hazardous, which makes it suitable for surgical applications [23]. It also has the benefit of being frictionless, compared to conventional cable-driven systems [24]. Magnetic catheters have been demonstrated to improve surgical efficiency through better control

during catheter guidance [25]. In this work, the actuation is achieved using an array of six electromagnetic coils called BigMag [26]. The coils can rotate around a spherical workspace with a diameter of approximately 10 cm. The system is capable of producing magnetic fields of specified magnitude and direction at any point within the workspace. Two cameras are also present in the setup which facilitate the sensing of the manipulator position and shape using stereo vision techniques.

The rest of the paper is laid out as follows. Section 2 details the derivation of the PRB model using screw theory, followed by the procedure for determining the optimal values of the PRB parameters in Section 3. The results of the optimization are tabulated, with explanations and preliminary validation. Section 4 describes the experimental setup to test the accuracy of the model and the results from the experiments. This is followed by a discussion of the contributions of the work, and ideas for improving the accuracy. The last section summarizes the key points of the work presented here, and also looks at some potential avenues for future work.

2. Pseudo-rigid-body model

In this section, a pseudo rigid body model is presented for determining the configuration of a flexible manipulator in three-dimensional space, under the influence of external loads. The manipulator analyzed here is assumed to undergo quasi-static motion, and has a large ratio of length to diameter with predominantly bending characteristics. The framework for deriving the model parameters and the method of analysis is generally applicable to manipulators with similar deformation behavior.

Fig. 2 shows a flexible manipulator in static equilibrium with loads ($\mathbf{W}_k \in \mathbb{R}^6$ ($k = 1, 2, 3$)) at points ($\mathbf{P}_k \in \mathbb{R}^3$) along its length, fixed at end \mathbf{P}_0 . Each segment (S_k) taken in isolation is in equilibrium with a load ($\mathbf{W} \in \mathbb{R}^6$) at its ends. In this paper, a PRB model with six degrees of freedom is used to approximate a given segment. The PRB model used here has four rigid links of a given length ($l_i \in \mathbb{R}^+$), connected by three joints, each with two degrees of freedom. Each joint (i) at point ($\mathbf{r}_i \in \mathbb{R}^3$) undergoes two angular deformations, first by angle ($\eta_i \in \mathbb{S}$) about the y -axis, followed by ($\theta_i \in \mathbb{S}$) about the z -axis. The rotational stiffness of each degree of freedom is defined by constants ($K_{\eta_i}, K_{\theta_i} \in \mathbb{R}^+$), corresponding to the respective joint angles (η_i, θ_i).

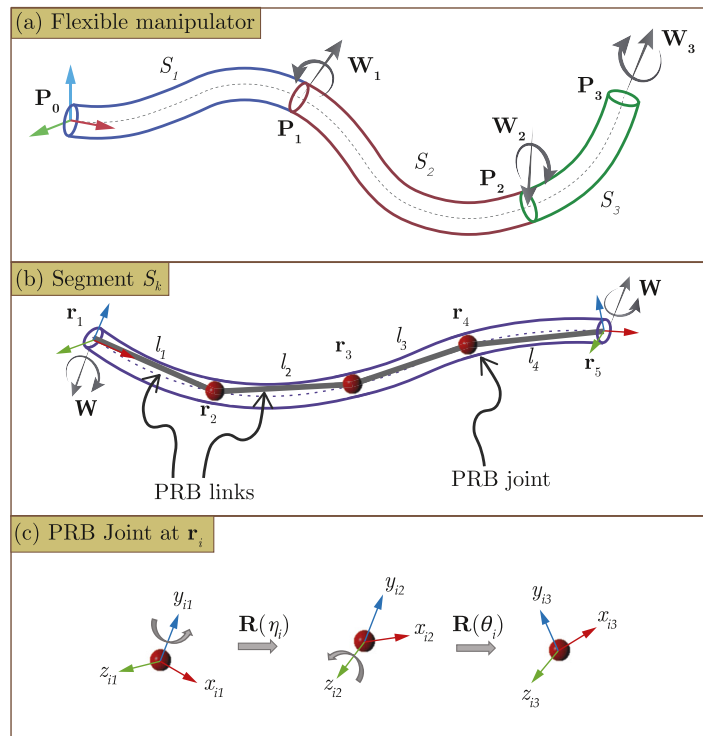


Fig. 2. A schematic of a 3D pseudo rigid body model for analysis of a flexible manipulator is shown. (a) The manipulator is fixed at one end ($\mathbf{P}_0 \in \mathbb{R}^3$), and deforms upon being subjected to loads ($\mathbf{W}_k \in \mathbb{R}^6$) at points ($\mathbf{P}_k \in \mathbb{R}^3$) ($k = 1, 2, 3$) along its length. The manipulator is partitioned into segments (S_1, S_2 and S_3) between two successive loads. (b) Each segment (S_k) is in static equilibrium with tip load ($\mathbf{W} \in \mathbb{R}^6$). Using the pseudo rigid body modeling approach, the segment can be replaced by a series of rigid links (with length of link (i) defined as $l_i \in \mathbb{R}^+$) connected by joints. In this work, a four-link pseudo rigid body model is used, with joints at $\mathbf{r}_i \in \mathbb{R}^3$ ($i = 1, 2, 3, 4, 5$). (c) There are two successive intrinsic rotations at each joint: first by an angle ($\eta_i \in \mathbb{S}$) about the y -axis, followed by an angle ($\theta_i \in \mathbb{S}$) about the z -axis (represented as $\mathbf{R}(\eta_i) \in \text{SO3}$ and $\mathbf{R}(\theta_i) \in \text{SO3}$, respectively).

The transformation from joint (i) to joint ($i + 1$), $\mathbf{T}_i^{i+1} \in \text{SE}(3)$ is given by

$$\mathbf{T}_i^{i+1} = \begin{bmatrix} c_{\eta_i} c_{\theta_i} & -c_{\eta_i} s_{\theta_i} & s_{\eta_i} & l_i \\ s_{\eta_i} c_{\theta_i} & c_{\theta_i} & 0 & 0 \\ -s_{\eta_i} c_{\theta_i} & s_{\eta_i} s_{\theta_i} & c_{\eta_i} & 0 \\ 0 & 0 & 0 & 1 \end{bmatrix}, \tag{1}$$

where s_* and c_* are the sine and cosine of angle ($*$), respectively. The coordinates of each joint (\mathbf{r}_i) are calculated as

$$\begin{bmatrix} \mathbf{r}_i \\ 1 \end{bmatrix} = \prod_{j=1}^{i-1} \mathbf{T}_j^{j+1} \cdot \begin{bmatrix} \mathbf{r}_1 \\ 1 \end{bmatrix}. \tag{2}$$

In the above equation, the angles related to the first joint (η_1 and θ_1) have zero magnitude since the first link is assumed to be rigidly fixed to the base frame.

The geometric twist between two successive degrees of freedom is calculated from the rotation axis ($\omega_* \in \mathbb{R}^3$) and the position vector ($q_* \in \mathbb{R}^3$). For joint (i),

$$\mathbf{q}_{\eta_i} = (l_{i-1} \quad 0 \quad 0)^T, \tag{3}$$

$$\mathbf{q}_{\theta_i} = (0 \quad 0 \quad 0)^T, \tag{4}$$

$$\omega_{\eta_i} = (0 \quad 1 \quad 0)^T, \tag{5}$$

$$\omega_{\theta_i} = (0 \quad 0 \quad 1)^T, \tag{6}$$

which allows us to define the associated twists ($\zeta_{\eta_i}, \zeta_{\theta_i} \in \mathbb{R}^6$) as

$$\zeta_{\eta_i} = \begin{bmatrix} \mathbf{q}_{\eta_i} \times \omega_{\eta_i} \\ \omega_{\eta_i} \end{bmatrix} = [0 \quad 0 \quad l_{i-1} \quad 0 \quad 1 \quad 0]^T, \tag{7}$$

$$\zeta_{\theta_i} = \begin{bmatrix} \mathbf{q}_{\theta_i} \times \omega_{\theta_i} \\ \omega_{\theta_i} \end{bmatrix} = [0 \quad 0 \quad 0 \quad 0 \quad 0 \quad 1]^T. \tag{8}$$

The spatial manipulator Jacobian is used to derive the statics equations for the PRB model [27]. The set of all the angles ($\Theta \in \mathbb{S}^6$) that define the configuration of the PRB model is

$$\Theta = [\eta_2, \theta_2, \eta_3, \theta_3, \eta_4, \theta_4]^T.$$

The Jacobian ($\mathbf{J}_\Theta \in \mathbb{R}^{6 \times 6}$) is given by

$$\mathbf{J}_\Theta = [\zeta'_{\eta_2} \quad \zeta'_{\theta_2} \quad \zeta'_{\eta_3} \quad \zeta'_{\theta_3} \quad \zeta'_{\eta_4} \quad \zeta'_{\theta_4}], \tag{9}$$

where

$$\zeta'_{\eta_i} = \text{Ad} \left(\mathbf{T}_1^2 \dots \mathbf{T}_{i-2}^{i-1} \Big|_{l_{i-1}=0} \right) \zeta_{\eta_i}, \tag{10}$$

$$\zeta'_{\theta_i} = \text{Ad} \left(\mathbf{T}_1^2 \dots \mathbf{T}_{i-1}^i \Big|_{\substack{\eta_i=0 \\ l_i=0}} \right) \zeta_{\theta_i}, \tag{11}$$

where $\text{Ad}(\mathbf{T})$ represents the adjoint transformation associated with the transformation matrix \mathbf{T} .

The set of internal torques in the PRB model ($\tau \in \mathbb{R}^6$) is represented as

$$\tau = [K_{\eta_i} \eta_i \quad K_{\theta_i} \theta_i] \quad i = 2, 3, 4. \tag{12}$$

The load wrench (\mathbf{W}) can be decomposed into a force ($\mathbf{F} \in \mathbb{R}^3$) and a moment ($\mathbf{M} \in \mathbb{R}^3$), and defined in the spatial reference frame as

$$\mathbf{W} = \begin{bmatrix} \mathbf{F} \\ \mathbf{M} \end{bmatrix} + \begin{bmatrix} 0_{3 \times 1} \\ \mathbf{r}_5 \times \mathbf{F} \end{bmatrix}. \tag{13}$$

The above definition of the external loads allows the inclusion of any form of actuation or contact that can be represented as a point load. The static behavior of the PRB model can be determined using the following equation.

$$\boldsymbol{\tau} = (\mathbf{J}_{\boldsymbol{\theta}})^T \mathbf{W}. \quad (14)$$

The above equation is a system of six nonlinear algebraic equations that can be solved to obtain the values of the six variables ($\eta_i, \theta_i : i = 2, 3, 4$) given any load wrench acting at the tip.

Eq. (14) can be extended to a system having multiple loads, such as the one shown in Fig. 2(a) with three loads acting on it. Each segment (S_k) can be replaced by the 6-DOF PRB model for analysis, with the ends of adjacent segments rigidly attached to one another. The statics equations for the system are given by

$$\begin{bmatrix} \boldsymbol{\tau}_1 \\ \boldsymbol{\tau}_2 \\ \boldsymbol{\tau}_3 \end{bmatrix} = \begin{bmatrix} (\mathbf{J}_{\boldsymbol{\theta}_1})^T & (\mathbf{J}_{\boldsymbol{\theta}_1})^T & (\mathbf{J}_{\boldsymbol{\theta}_1})^T \\ 0 & (\mathbf{J}_{\boldsymbol{\theta}_2})^T & (\mathbf{J}_{\boldsymbol{\theta}_2})^T \\ 0 & 0 & (\mathbf{J}_{\boldsymbol{\theta}_3})^T \end{bmatrix} \begin{bmatrix} \mathbf{W}_1 \\ \mathbf{W}_2 \\ \mathbf{W}_3 \end{bmatrix}, \quad (15)$$

where $\mathbf{J}_{\boldsymbol{\theta}_k}$ is the Jacobian matrix associated with segment S_k , and $\boldsymbol{\tau}_k$ is the corresponding set of internal torques.

3. Parameter optimization

In this section, the values of the constant PRB parameters (l_i, K_{η_i} and K_{θ_j}) are determined using an optimization process. This is accomplished using data obtained from other controlled and verifiable methods, such as high-fidelity simulations (theoretical data) and experiments (empirical data). Once the parameter values for a single PRB segment are calculated using this approach, manipulators of similar materials and geometries can be modeled using the same parameters. The optimal parameter values for the single segment model are used in Section 4 to analyze a manipulator with multiple loads exerted on it.

3.1. Optimization framework

The PRB parameters are defined with dimensionless variables as given below.

$$l_i = \gamma_i L \quad (16)$$

$$K_{\eta_j} = k_{\eta_j} \frac{EI}{L}, \quad (17)$$

$$K_{\theta_j} = k_{\theta_j} \frac{EI}{L}, \quad (18)$$

where $i = 1, 2, 3, 4$, $j = 2, 3, 4$, EI represents the flexural rigidity (product of elastic modulus and area moment of inertia) and L is the length of the manipulator segment. This allows the model to be extended to similar manipulators by using appropriate material properties and geometric dimensions.

The optimization process calculates the best values of the PRB parameters so that the model closely matches the deformation behavior of the manipulator segment. From the verifiable data, a set of N static loading cases is extracted to be used as the basis for optimization [28]. The error of the PRB model in modeling a specific loading case (k) is defined as

$$e_k = \|\mathbf{Y}_k - \mathbf{Y}_k^{PRB}\|, \quad (19)$$

where \mathbf{Y}_k^{PRB} is the coordinates of the tip (\mathbf{r}_5) calculated using the PRB model, and the corresponding results from the verifiable data are represented by \mathbf{Y}_k . If \mathbf{X} is the set of PRB parameters to be optimized, the optimization problem can be defined as

$$\begin{aligned} \text{Minimize} \quad & f(\mathbf{X}) = \frac{1}{N} \sum_{k=1}^N e_k, \\ \text{where} \quad & \mathbf{X} = \{\gamma_i, k_{\eta_j}, k_{\theta_j}\}, \\ & i = 1, 2, 3, 4 \quad j = 2, 3, 4 \\ \text{subject to} \quad & \mathbf{X}_{lb} \leq \mathbf{X} \leq \mathbf{X}_{ub}, \\ & \sum_{i=1}^4 \gamma_i = 1, \end{aligned} \quad (20)$$

where \mathbf{X}_{lb} and \mathbf{X}_{ub} are the lower and upper bounds of the variables under optimization, respectively.

In this work, the model is defined to be symmetric about the middle joint (\mathbf{r}_3), which has two advantages. Firstly, it reduces the number of variables in the optimization, and secondly, it allows the implementation of boundary conditions at

Table 1

Optimal values of dimensionless pseudo rigid body model parameters for minimizing the model error based on data from Finite Element Analysis. The parameters relate to the length of the pseudo rigid body segment ($l_1 = \gamma_1 L$, where L is the length of the manipulator segment) and stiffness of the joints ($K_{\eta_j} = k_{\eta_j} \frac{EI}{L}$, $K_{\theta_j} = k_{\theta_j} \frac{EI}{L}$, $j = 2, 3$, where E is the elastic modulus and I is the second moment of area of the cross section of the manipulator). The optimization is performed over $N = 7776$ data points as described in Section 3.2. The average error in estimating the tip position is 0.98% of the manipulator length.

γ_1	k_{η_2}	k_{η_3}	k_{θ_2}	k_{θ_3}
0.1699	2.5064	4.8339	2.4914	5.0303

either end without affecting the analysis. This leads to the following relations.

$$\gamma_1 = \gamma_4 \quad (21)$$

$$k_{\eta_2} = k_{\eta_4} \quad (22)$$

$$k_{\theta_2} = k_{\theta_4} \quad (23)$$

$$\gamma_2 = \gamma_3 = 0.5 - \gamma_1. \quad (24)$$

Therefore, there are five independent PRB parameters to be determined, namely γ_1 , k_{η_2} , k_{η_3} , k_{θ_2} and k_{θ_3} . The optimization was performed using the function `fmincon` in MATLAB (Version 9.2.0.556344, Mathworks Inc., Natick, Massachusetts, U.S.A.).

3.2. Validation with finite element analysis

The proposed method using the PRB model is first validated using FEA. A continuum manipulator is modeled in Ansys Workbench (Version 16.2, Ansys Inc., Canonsburg, Pennsylvania, U.S.A.) using BEAM188 elements (2-node beam element in 3D) of 1 mm length. The optimization of the PRB parameters is initially performed for a single segment. Force and moment loads are applied at the tip of the manipulator, while the other end is fixed. The maximum and minimum values of the forces (F_x , F_y , F_z) are -4mN and 4mN , respectively, while those for the moments (M_y , M_z) are -250 mN mm and 250 mN mm , respectively. Torsional moments (M_x) are not applied. A total of $N = 7776$ data points are obtained for a manipulator of length 50 mm, with an elastic modulus (E) of 350 MPa and a bending moment of inertia (I) of $4.91 \times 10^{-2}\text{ mm}^4$.

The framework described in Section 3.1 is used to determine the optimal values of the PRB parameters, which are given in Table 1. The average error in estimation of the tip position by the model compared to the FEA data is 0.488 mm (less than 1% of the manipulator length). Four deflected positions of the manipulator and the corresponding PRB model are shown in Fig. 3.

The same parameter values are then used to analyze a manipulator with multiple segments. Point loads are applied at specific positions along a length of 110 mm. The multi-segment model described in Eq. (15) is used to analyze the system, and the results from the PRB model and FEA are plotted in Fig. 4. The plot shows good agreement between the two sets of results, and the shape of the manipulator is estimated by the PRB model by an mean error of 0.36 mm along its length across the three loading cases. These results demonstrate that once the optimal PRB parameters for a single segment are determined, they can be used for similar manipulators of different lengths subjected to multiple loads.

4. Experiments and results

In this section, a magnetically-actuated surgical catheter is used to illustrate the application of the PRB model through experiments. At first, the PRB parameters are optimized for a segment with point loads at its free end, and then the same values are used to predict the deformation of a similar device in a multiple-load scenario.

4.1. Experiment setup

The experiments are performed using an array of electromagnetic coils (BigMag [26]). The manipulator is a hollow tube (diameter $\phi_{outer} = 2\text{ mm}$, $\phi_{inner} = 1.2\text{ mm}$) made of an elastomer (PEBAX 6663). Four Neodymium ring magnets (height $h = 2\text{ mm}$, diameter $\phi_{outer} = 6\text{ mm}$, $\phi_{inner} = 2\text{ mm}$, and mass $m = 0.38\text{ g}$) are attached to the tip of the tube. The magnetic dipole ($\boldsymbol{\mu} \in \mathbb{R}^3$, $|\boldsymbol{\mu}| = 0.176\text{ A/m}^2$) acts along the axis of the ring magnets. The electromagnet coil array is capable of producing a specified magnetic field ($\mathbf{B}_m \in \mathbb{R}^3$) at the tip of the manipulator. The field produces a force ($\mathbf{F}_\mu \in \mathbb{R}^3$) and a moment

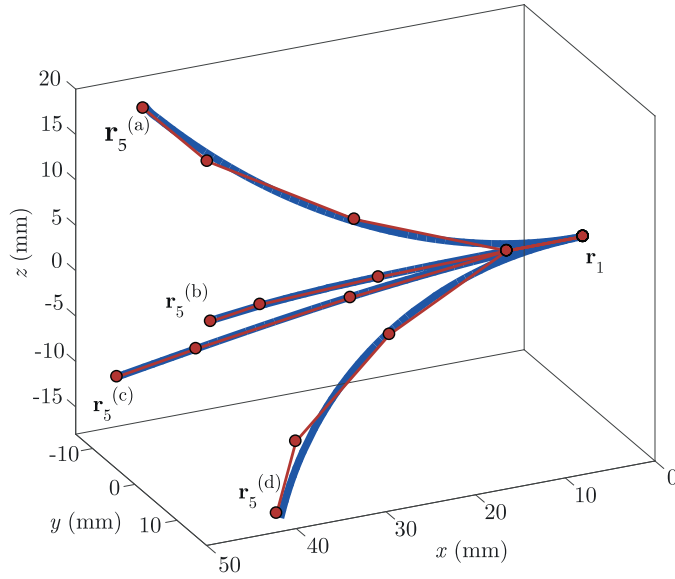


Fig. 3. Comparison of optimized pseudo rigid body model (red) to manipulator shape from Finite Element Analysis (blue) calculated using Ansys Workbench (Version 16.2, Ansys Inc., Canonsburg, Pennsylvania, U.S.A.) for a single segment with tip loads. Four example configurations are shown (a, b, c, d). The manipulator is fixed at \mathbf{r}_0 and loads are applied at the tip locations (\mathbf{r}_5^*). The length of the undeformed manipulator is 50 mm. The tip loads in the different configurations are: (a) $\mathbf{F} = (4, -2.5, 2.5)$ mN, $\mathbf{M} = (0, -250, -150)$ mN mm, (b) $\mathbf{F} = (-4, -4, -4)$ mN, $\mathbf{M} = (0, 0, 0)$ mN mm, (c) $\mathbf{F} = (0, 1, 2)$ mN, $\mathbf{M} = (0, 0, 150)$ mN mm, (d) $\mathbf{F} = (-3, 1, 0)$ mN, $\mathbf{M} = (0, 200, -100)$ mN mm. (For interpretation of the references to colour in this figure legend, the reader is referred to the web version of this article.)

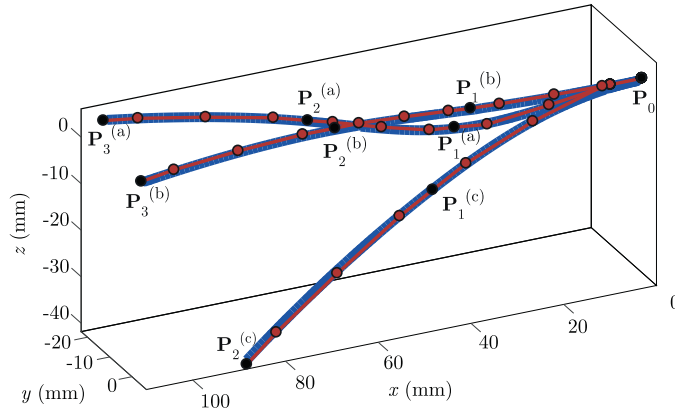


Fig. 4. Comparison of optimized pseudo rigid body model (red) to manipulator shape from Finite Element Analysis (blue) for multiple external loads. Three example configurations are shown (a, b, c). The manipulator is fixed at \mathbf{P}_0 and the locations of the loads are marked \mathbf{P}_1^* , \mathbf{P}_2^* and \mathbf{P}_3^* . The length of the undeformed manipulator is 110 mm. The loads applied in the various configurations are: (a) : $\mathbf{F}_1 = (0, 5.15, 0)$ mN, $\mathbf{F}_2 = (0, 0, 4.91)$ mN, $\mathbf{F}_3 = (0, 0, -1)$ mN, $\mathbf{M}_3 = (0, 100, -100)$ mN mm, (b) : $\mathbf{F}_1 = (0, 2.69, -2.66)$ mN, $\mathbf{F}_2 = (0, 0, -15.0)$ mN, $\mathbf{F}_3 = (0, 0, -1)$ mN, $\mathbf{M}_3 = (0, 100, -100)$ mN mm, (c) : $\mathbf{F}_1 = (0, 5.15, 0)$ mN, $\mathbf{F}_2 = (0, 0, -1)$ mN, $\mathbf{M}_2 = (0, 100, -100)$ mN mm. Note that configuration (c) has only two points of loading. (For interpretation of the references to colour in this figure legend, the reader is referred to the web version of this article.)

($\mathbf{M}_\mu \in \mathbb{R}^3$) given by

$$\mathbf{F}_\mu = \nabla(\boldsymbol{\mu} \cdot \mathbf{B}_m) \quad (25)$$

$$\mathbf{M}_\mu = \boldsymbol{\mu} \times \mathbf{B}_m \quad (26)$$

where $\boldsymbol{\mu}$ is aligned with the axis of the manipulator tip. The mass of the magnets also produces a gravity force ($\mathbf{F}_g = m\mathbf{g} \in \mathbb{R}^3$) at the same point ($\mathbf{g} \in \mathbb{R}^3$ is the acceleration due to gravity). The mass of the manipulator is neglected since it is significantly smaller than that of the magnets.

The total force and moment at the manipulator tip (as defined in Eq. (13)) are given by

$$\mathbf{F} = \mathbf{F}_\mu + \mathbf{F}_g \quad (27)$$

$$\mathbf{M} = \mathbf{M}_\mu \quad (28)$$

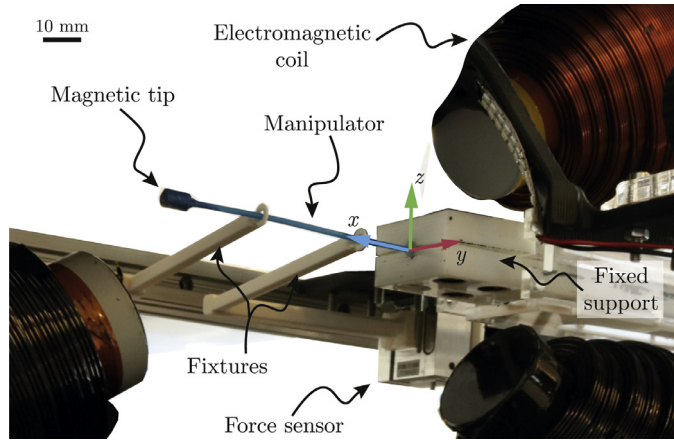


Fig. 5. The experimental setup for validating the pseudo rigid body model, with a continuum manipulator actuated by an array of six electromagnetic coils (three are shown). The manipulator is fixed at one end (directions of the axes at the base frame are shown) and permanent magnets are attached to the other end. Fixtures are used to enforce displacement constraints for simulating a manipulator with environmental loads. The contact forces between the fixtures and the manipulator are measured using two three-axis force sensors (one is not in frame). The shape of the manipulator is captured in the xy - and xz - planes using cameras.

Table 2

Minimum and maximum values of magnetic forces and moments applied to manipulator tip when collecting data for optimization of the pseudo rigid body model. The load values are calculated using Eqs. (25) and (26) in the fixed spatial reference frame, with knowledge of the applied magnetic field and the direction of the magnetic dipole at the tip of the manipulator.

	F_{μ}^x (mN)	F_{μ}^y (mN)	F_{μ}^z (mN)
Minimum	-11.1	-55.2	-23.9
Maximum	9.46	27.9	30.4
	M_{μ}^x (mN mm)	M_{μ}^y (mN mm)	M_{μ}^z (mN mm)
Minimum	-270.4	-1735.5	-1687.4
Maximum	355.6	1630.1	1809.7

Table 3

Optimal values of dimensionless pseudo rigid body model parameters for minimizing the model error based on experimental data. The parameters relate to the length of the pseudo rigid body segment ($l_1 = \gamma_1 L$, where L is the length of the manipulator segment) and stiffness of the joints ($K_{\eta_j} = k_{\eta_j} \frac{EI}{L}$, $K_{\theta_j} = k_{\theta_j} \frac{EI}{L}$, $j = 2, 3$, where EI represents the flexural rigidity of the manipulator). The optimization is performed over $N = 360$ data points as described in Section 4.1.

γ_1	k_{η_2}	k_{η_3}	k_{θ_2}	k_{θ_3}
0.1184	1.8895	5.6053	2.0106	5.0667

and is used to actuate the manipulator. The experimental setup is shown in Fig. 5. The manipulator shape is tracked with a stereo vision system and reconstructed using a technique similar to the one described by Camarillo et al. [29].

4.2. Optimization results

The magnetic setup described above is used to generate a set of data for determining the PRB parameters for a single manipulator segment of length 52 mm. The magnetic field is applied to obtain deflected manipulator configurations using vision-based tracking from the cameras, and data (magnetic field and manipulator shape for $N = 360$ points) is collected. The range of loads used in the experiment is given in Table 2. The optimization framework is applied to fit the model and the resulting PRB parameter values are given in Table 3. The optimized PRB model estimates the position of the manipulator tip with an error of 2.2 ± 1.76 mm over the entire range of data. The high standard deviation arises from error at a few data points where the magnet is close to the electromagnetic coils (very large forces). The accuracy of the model is also illustrated through four representative manipulator configurations in Fig. 6.

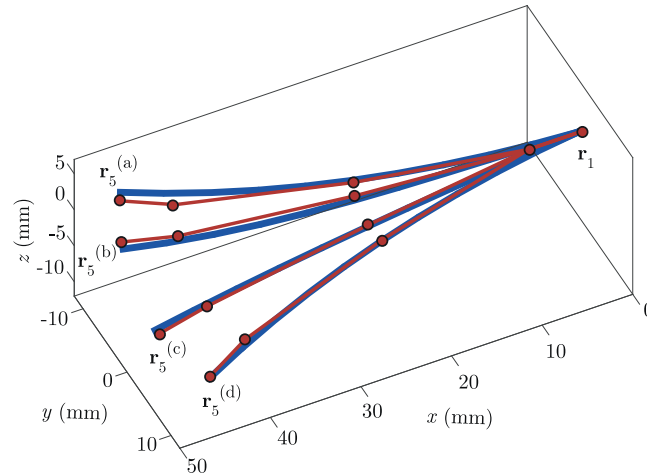


Fig. 6. Comparison of optimized pseudo rigid body model (red) to manipulator shape from experiments (blue) for a single segment with tip loads. Four example configurations are shown (a, b, c and d). The manipulator is fixed at \mathbf{r}_1 and loads are applied at the tip locations (\mathbf{r}_5^* , where * is (a), (b), (c) or (d)). The length of the undeformed manipulator is 52 mm. The tip loads in the different configurations are: (a) $\mathbf{F} = (1.27, 0.21, -1.62)$ mN, $\mathbf{M} = (-1580, -780, -1360)$ mN mm, (b) $\mathbf{F} = (1.27, 0.83, -0.14)$ mN, $\mathbf{M} = (-160, 0, -1330)$ mN mm, (c) $\mathbf{F} = (-0.10, 1.43, -0.08)$ mN, $\mathbf{M} = (0, 510, 0)$ mN mm, (d) $\mathbf{F} = (-4.32, -3.77, -6.07)$ mN, $\mathbf{M} = (210, 0, 1500)$ mN mm. (For interpretation of the references to colour in this figure legend, the reader is referred to the web version of this article.)

4.3. Multi-load experiments

In this section, the application of the optimized PRB model for the analysis of a manipulator subjected to multiple loads is demonstrated. Similar to Fig. 2(a), the manipulator is fixed at one end \mathbf{P}_0 and actuated by magnetic loads and gravity at end \mathbf{P}_3 . Two displacement constraints are applied at points \mathbf{P}_1 and \mathbf{P}_2 , leading to reaction forces \mathbf{F}_1 and \mathbf{F}_2 . It is assumed that there are no moment reactions since there are no orientation constraints. Here, the analysis involves calculating the reaction forces and the manipulator shape, when the actuation loads and position of displacement constraints are known. If \mathbf{F}_3 , \mathbf{M}_3 , \mathbf{P}_1 and \mathbf{P}_2 are known, the PRB angles ($\Theta_i, i = 1, 2, 3$), and the forces (\mathbf{F}_1 and \mathbf{F}_2) can be determined using Eqs. (2) and (15), a system of 24 equations in as many unknowns. The equations were solved using `fsolve` function in MATLAB (Version 9.2.0.556344).

The displacement constraints are applied using two fixtures, which are designed to constrain the manipulator only in the lateral direction (y and z axes), while allowing slippage in the axial direction (x axis). Due to this, the x -component of the reaction forces is assumed to be zero for the analysis. The fixtures are printed using acrylonitrile butadiene styrene (ABS) and are attached to three-axis force sensors (Model number: K3D40 from ME-Meßsysteme GmbH, Hennigsdorf, Germany). The total length of the manipulator for this experiment is 82 mm. The locations of the constraints (\mathbf{P}_1 and \mathbf{P}_2) are calculated when the magnetic field is zero.

The experiment was run for 169 values of the actuation load, and the shape and force data were recorded. The forces were also estimated using the PRB model as described above (with the parameter values in Table 3), and the values obtained from the model were compared against those from the experiment in Fig. 7. The mean error in estimating the reaction forces was 140 mN and 27 mN for the y and z components of \mathbf{F}_1 , and 45 mN and 32 mN for \mathbf{F}_2 .

The shape of the manipulator as defined by the PRB model was determined using 3D splines. The splines were then compared against the recorded shape data from the cameras at 25 points along the length of the manipulator. For a given frame (i), the error in shape estimation ($e_i^s \in \mathbb{R}^+$) using the PRB model is calculated as

$$e_i^s = \sum_{k=1}^{25} \|\mathbf{r}_{i,k}^E - \mathbf{r}_{i,k}^P\| \quad (29)$$

where $\mathbf{r}_{i,k}^E \in \mathbb{R}^3$ and $\mathbf{r}_{i,k}^P \in \mathbb{R}^3$ refer to the coordinates of the points obtained from experiment and PRB model, respectively. The mean error in estimating the shape along the manipulator length was 1.2 ± 0.23 mm, also shown as a histogram in Fig. 8. The PRB model is plotted against the deformed manipulator configurations for two frames in Fig. 9.

4.4. Discussion

The error in estimation of the y -component of \mathbf{F}_1 is higher than others, which could be because the force is outside the range of loads used for the parameter optimization. The errors could also be due to deformation of the fixtures during the experiment, which means the displacement constraints are not maintained perfectly. For the manipulator shape, it was noticed that a major portion of the error was in the first PRB segment (between \mathbf{P}_0 and \mathbf{P}_1) due to the manipulator not

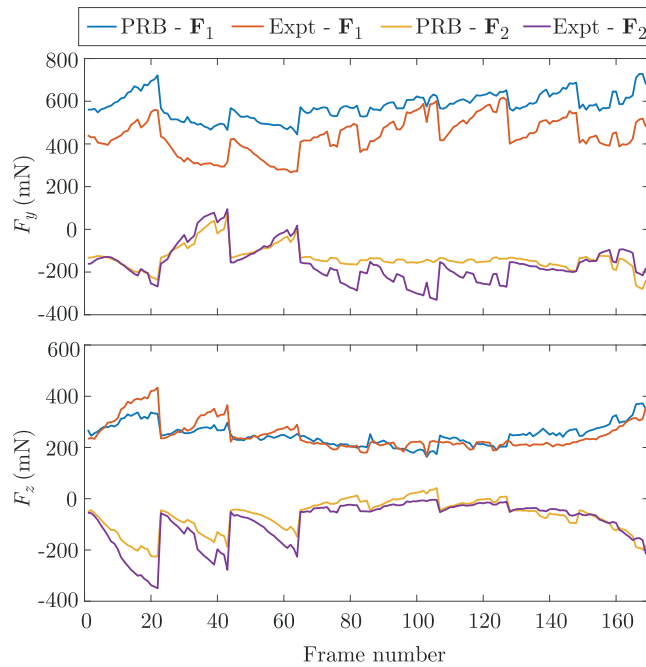


Fig. 7. Comparison of constraint forces obtained from experiments (Expt) to those calculated using the pseudo rigid body model (PRB). Displacement constraints are applied at two points along the length of the manipulator, and the corresponding reaction forces are named F_1 and F_2 . The top plot shows the forces in the direction of the y -axis (horizontal plane), and the bottom one shows the force in the direction of the z -axis (vertical plane). (For interpretation of the references to colour in this figure legend, the reader is referred to the web version of this article.)

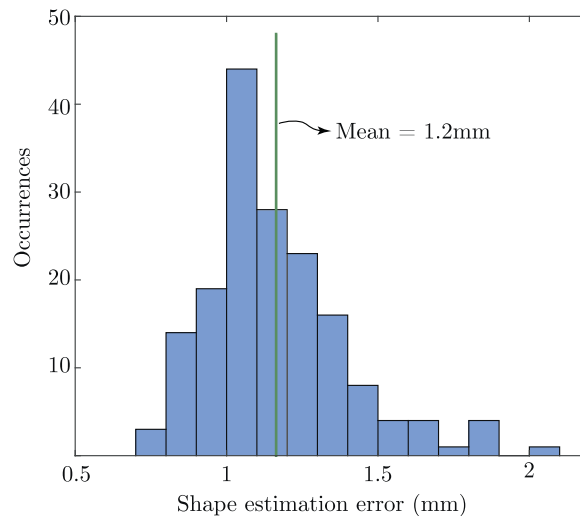
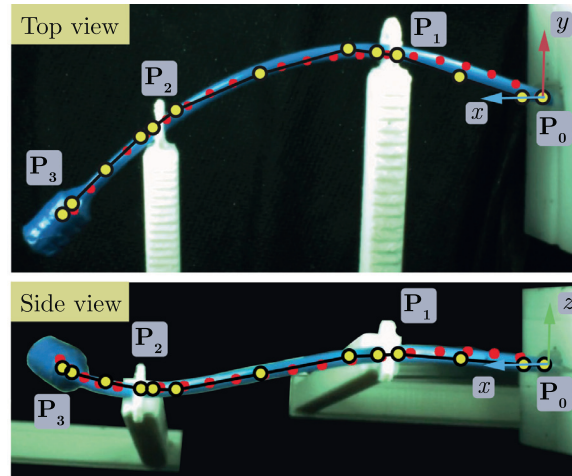


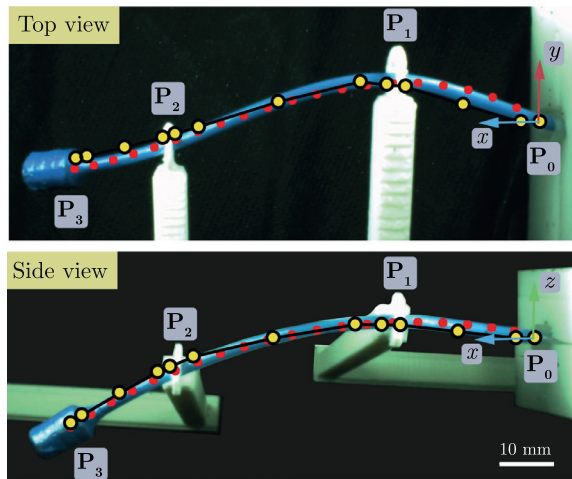
Fig. 8. A histogram of the error in shape estimation of the manipulator by the PRB model under multiple loads. The chart denotes the average distance between a spline through the PRB points and the tracking data obtained from experiments, across 169 occurrences.

being fully constrained at the base. It is also noticeable in Fig. 9 that the red dots obtained from the stereo-vision tracking system do not follow the shape of the manipulator perfectly, especially close to the fixed base. In spite of these issues, the estimated reaction forces and deformed shapes are close to the experimental results. The estimation of contact forces described here requires knowledge of the positions of the constraints (P_1 and P_2), which may not be readily available during application. If the manipulator is enclosed in a conduit, this can be addressed by providing the shape of the conduit and restricting the shape of the manipulator to stay within the permitted volume.

It is possible to increase the number of segments to achieve higher accuracy, but that will require a trade-off with computation time (In the work shown here, the single PRB model takes 6.8 ms while the combined model with external forces requires 174.5 ms on average for one calculation on a 8GB, 3.60GHz Intel i7 machine running Windows 10). Nonlinear



(a) Frame 40



(b) Frame 97

Fig. 9. The shape of the manipulator calculated using the pseudo rigid body model (black lines with yellow circles) is overlaid with the photographs from experiment. The manipulator (in blue) is fixed at P_0 and displacement constraints are applied at P_1 and P_2 using the supports shown in white. The forces at these points are measured using two 3-axis force sensors (not shown). The manipulator is divided into three segments, and each segment is approximated by a PRB model with four rigid links. The red dots are used to define a polynomial curve for the manipulator shape, obtained using a tracking method similar to Ref. [29]. The magnetic tip is at P_3 and is actuated by an external magnetic field using an array of electromagnetic coils. The results of two instances of the experiment are shown, corresponding to frames 40 and 97 in Fig. 7. (For interpretation of the references to colour in this figure legend, the reader is referred to the web version of this article.)

spring stiffnesses can be introduced if the accuracy using linear springs is considered to be insufficient. A larger pool of data for optimization will also help in reducing error. The model can also incorporate more complex behavior—for instance, a manipulator with an initial curvature can be defined with non-zero equilibrium angles. Twisting, shear and extension effects can also be integrated using suitable mechanical elements. Gravity has been included as a point load at the tip, but a distributed load profile can also be introduced with a bias in the vertical plane of the model.

5. Conclusions and future work

In this study, a framework is presented for the analysis of continuum manipulators using PRB models under quasi-static conditions. The method is applied for estimating the reaction forces and shape of a manipulator subjected to environmental constraints. An optimized PRB model is developed for a single segment, and the same parameter values are used for analyzing a manipulator with multiple loads exerted on it. The model shows good agreement with experiments in estimating the forces (61 mN mean error) and predicting the deformed shape of the manipulator (1.2 mm error in shape along length), while allowing for fast computation. While the PRB model is not derived from fundamental principles of elastic

rods, the adaptability of the optimization approach allows the same framework to be used for various types of continuum manipulators.

In the future, this approach will be applied to model the interaction of a manipulator with its environment, and extended to closed-loop control of manipulator motion. The use of the model for transient analysis and time-varying loads will also be studied. The model can also be combined with other sensing modalities, such as Fiber Bragg Grating Sensors (FBGS) or ultrasound scanning to be used for surgical applications.

Acknowledgements

This research has received funding from the [European Research Council](#) (ERC) under the European Unions [Horizon 2020](#) Research and Innovation programme (grant agreement #638428 - project ROBOTAR).

References

- [1] A.A. Transth, K.Y. Pettersen, P. Liljebck, A survey on snake robot modeling and locomotion, *Robotica* 27 (7) (2009) 999–1015, doi:[10.1017/S0263574709005414](#).
- [2] L. Margheri, C. Laschi, B. Mazzolai, Soft robotic arm inspired by the octopus: i. from biological functions to artificial requirements, *Bioinspir. Biomim.* 7 (2) (2012) 025004, doi:[10.1088/1748-3182/7/2/025004](#).
- [3] J. Burgner-Kahrs, D.C. Rucker, H. Choset, Continuum robots for medical applications: a survey, *IEEE Trans. Robotics* 31 (6) (2015) 1261–1280, doi:[10.1109/TRO.2015.2489500](#).
- [4] C. Majidi, Soft robotics: a perspective – current trends and prospects for the future, *Soft Robotics* 1 (1) (2013) 5–11, doi:[10.1089/soro.2013.0001](#).
- [5] R.J. Webster, B.A. Jones, Design and kinematic modeling of constant curvature continuum robots: a review, design and kinematic modeling of constant curvature continuum robots: a review, *Int. J. Robotics Res.* 29 (13) (2010) 1661–1683, doi:[10.1177/0278364910368147](#).
- [6] K. Xu, N. Simaan, Analytic formulation for kinematics, statics, and shape restoration of multibackbone continuum robots via elliptic integrals, *J. Mech. Robotics* 2 (1) (2010) 011006, doi:[10.1115/1.4000519](#).
- [7] D. Trivedi, A. Lotfi, C.D. Rahn, Geometrically exact models for soft robotic manipulators, *IEEE Trans. Robotics* 24 (4) (2008) 773–780, doi:[10.1109/TRO.2008.924923](#).
- [8] D.C. Rucker, B.A. Jones, R.J. Webster, A geometrically exact model for externally loaded concentric-tube continuum robots, *IEEE Trans. Robotics* 26 (5) (2010) 769–780, doi:[10.1109/TRO.2010.2062570](#).
- [9] W. Tang, T.R. Wan, D.A. Gould, T. How, N.W. John, A stable and real-time nonlinear elastic approach to simulating guidewire and catheter insertions based on Cosserat rod, *IEEE Trans. Biomed. Eng.* 59 (8) (2012) 2211–2218, doi:[10.1109/TBME.2012.2199319](#).
- [10] J. Till, C.E. Bryson, S. Chung, A.L. Orekhov, D.C. Rucker, Efficient computation of multiple coupled Cosserat rod models for real-time simulation and control of parallel continuum manipulators, in: 2015 IEEE International Conference on Robotics and Automation (ICRA), 2015, pp. 5067–5074, doi:[10.1109/ICRA.2015.7139904](#).
- [11] H. Mochiyama, Model validation of discretized spatial closed elastica, in: 2016 IEEE/RSJ International Conference on Intelligent Robots and Systems (IROS), 2016, pp. 5216–5223, doi:[10.1109/IROS.2016.7759767](#).
- [12] J. Back, T. Manwell, R. Karim, K. Rhode, K. Althoefer, H. Liu, Catheter contact force estimation from shape detection using a real-time Cosserat rod model, in: 2015 IEEE/RSJ International Conference on Intelligent Robots and Systems (IROS), 2015, pp. 2037–2042, doi:[10.1109/IROS.2015.7353647](#).
- [13] E. Coevoet, A. Escande, C. Duriez, Optimization-based inverse model of soft robots with contact handling, *IEEE Robotics Autom. Lett.* 2 (3) (2017) 1413–1419, doi:[10.1109/LRA.2017.2669367](#).
- [14] Z. Zhang, J. Dequidt, J. Back, H. Liu, C. Duriez, Motion control of cable-driven continuum catheter robot through contacts, *IEEE Robotics Autom. Lett.* 4 (2) (2019) 1852–1859, doi:[10.1109/LRA.2019.2898047](#).
- [15] L.L. Howell, *Compliant Mechanisms*, John Wiley & Sons, New York, NY, 2001.
- [16] V.K. Venkiteswaran, O.A. Turkan, H.-J. Su, Speeding up topology optimization of compliant mechanisms with a pseudorigid-body model, *J. Mech. Robotics* 9 (4) (2017) 041007, doi:[10.1115/1.4035992](#).
- [17] M. Khoshnam, R.V. Patel, A pseudo-rigid-body 3r model for a steerable ablation catheter, in: 2013 IEEE International Conference on Robotics and Automation, 2013, pp. 4427–4432, doi:[10.1109/ICRA.2013.6631205](#).
- [18] T. Greigarn, M.C. Çavuşoğlu, Pseudo-rigid-body model and kinematic analysis of MRI-actuated catheters, in: 2015 IEEE International Conference on Robotics and Automation (ICRA), 2015, pp. 2236–2243, doi:[10.1109/ICRA.2015.7139495](#).
- [19] T. Greigarn, R. Jackson, T. Liu, M.C. Çavuşoğlu, Experimental validation of the pseudo-rigid-body model of the MRI-actuated catheter, in: 2017 IEEE International Conference on Robotics and Automation (ICRA), 2017, pp. 3600–3605, doi:[10.1109/ICRA.2017.7989414](#).
- [20] R.J. Roesthuis, S. Misra, Steering of multisegment continuum manipulators using rigid-link modeling and FBG-based shape sensing, *IEEE Trans. Robotics* 32 (2) (2016) 372–382, doi:[10.1109/TRO.2016.2527047](#).
- [21] S. Huang, D. Meng, Y. She, X. Wang, B. Liang, B. Yuan, Statics of continuum space manipulators with nonconstant curvature via pseudorigid-body 3r model, *IEEE Access* 6 (2018) 70854–70865, doi:[10.1109/ACCESS.2018.2881261](#).
- [22] J. Edelmann, A.J. Petruska, B.J. Nelson, Magnetic control of continuum devices, *Int. J. Robotics Res.* 36 (1) (2017) 68–85.
- [23] C. Heunis, J. Sikorski, S. Misra, Improved magnetic steering, actuation, and image-guided surgical instruments, *IEEE Robotics Autom. Mag.* 1070 (9932/18) (2018) 2.
- [24] G. Tholey, J.P. Desai, A.E. Castellanos, Force feedback plays a significant role in minimally invasive surgery, *Annals Surgery* 241 (1) (2005) 102–109, doi:[10.1097/01.sla.0000149301.60553.1e](#).
- [25] S. Ernst, Initial experience with remote catheter ablation using a novel magnetic navigation system: magnetic remote catheter ablation, *Circulation* 109 (12) (2004) 1472–1475, doi:[10.1161/01.CIR.0000125126.83579.1B](#).
- [26] J. Sikorski, I. Dawson, A. Denasi, E.E.G. Hekman, S. Misra, Introducing BigMag – a novel system for 3d magnetic actuation of flexible surgical manipulators, in: 2017 IEEE International Conference on Robotics and Automation (ICRA), 2017, pp. 3594–3599, doi:[10.1109/ICRA.2017.7989413](#).
- [27] R.M. Murray, Z. Li, S.S. Sastry, S.S. Sastry, *A Mathematical Introduction to Robotic Manipulation*, CRC Press, 1994.
- [28] V.K. Venkiteswaran, H.-J. Su, A parameter optimization framework for determining the pseudo-rigid-body model of cantilever-beams, *Precis. Eng.* 40 (2015) 46–54, doi:[10.1016/j.precisioneng.2014.10.002](#).
- [29] D.B. Camarillo, K.E. Loewke, C.R. Carlson, J.K. Salisbury, Vision based 3-d shape sensing of flexible manipulators, in: *Robotics and Automation, 2008. ICRA 2008. IEEE International Conference on*, IEEE, 2008, pp. 2940–2947.